

Journal Pre-proof

Substituted benzothiophene and benzofuran derivatives as a novel class of bone morphogenetic Protein-2 upregulators: Synthesis, anti-osteoporosis efficacies in ovariectomized rats and a zebrafish model, and ADME properties

Si-tu Xue, Lei Zhang, Zhuo-song Xie, Jie Jin, Hui-Fang Guo, Hong Yi, Zong-ying Liu, Zhuo-rong Li

PII: S0223-5234(20)30436-0

DOI: <https://doi.org/10.1016/j.ejmech.2020.112465>

Reference: EJMECH 112465

To appear in: *European Journal of Medicinal Chemistry*

Received Date: 9 March 2020

Revised Date: 28 April 2020

Accepted Date: 12 May 2020

Please cite this article as: S.-t. Xue, L. Zhang, Z.-s. Xie, J. Jin, H.-F. Guo, H. Yi, Z.-y. Liu, Z.-r. Li, Substituted benzothiophene and benzofuran derivatives as a novel class of bone morphogenetic Protein-2 upregulators: Synthesis, anti-osteoporosis efficacies in ovariectomized rats and a zebrafish model, and ADME properties, *European Journal of Medicinal Chemistry* (2020), doi: <https://doi.org/10.1016/j.ejmech.2020.112465>.

This is a PDF file of an article that has undergone enhancements after acceptance, such as the addition of a cover page and metadata, and formatting for readability, but it is not yet the definitive version of record. This version will undergo additional copyediting, typesetting and review before it is published in its final form, but we are providing this version to give early visibility of the article. Please note that, during the production process, errors may be discovered which could affect the content, and all legal disclaimers that apply to the journal pertain.

© 2020 Published by Elsevier Masson SAS.



Substituted Benzothiophene and Benzofuran Derivatives as a Novel Class of Bone Morphogenetic Protein-2 Upregulators: Synthesis, Anti-osteoporosis Efficacies in Ovariectomized Rats and a Zebrafish Model, and ADME Properties

Si-tu Xue[†], Lei Zhang[†], Zhuo-song Xie, Jie Jin, Hui-Fang Guo, Hong Yi, Zong-ying Liu, Zhuo-rong Li**

Institute of Medicinal Biotechnology, Chinese Academy of Medical Sciences & Peking Union Medical College, Beijing 100050, China

ABSTRACT

The bone morphogenetic protein (BMP) pathway is a promising new target for the design of therapeutic agents for the treatment of low bone mass. This study optimized the structure of the anti-osteoporosis compound **38** by balancing its lipophilicity and improving its stability. Twenty derivatives which were not reported in the literature were designed and synthesized. The ovariectomized rat model of osteoporosis was selected to evaluate the therapeutic effects. Compound **125** showed better therapeutic efficacy than that of **38**. We verified the anti-osteoporosis activity and BMP-2 protein upregulation after treatment with **125** in a zebrafish

osteoporosis model. We found that **125** improved the ADME properties, therapeutic efficacy, and pharmacokinetics of the drug. Overall, we evaluated the anti-osteoporosis effects of the compounds of this type, preliminarily determined the target patient population, verified the mechanism of action, clarified the level of toxicity, and provided preliminary ADME data. We believe that these compounds can both correct bone loss that is already occurring in patients and have broad clinical applicability.

KEYWORDS

Bone morphogenetic protein-2, Osteoporosis, Osteogenesis, Benzothiophene, Benzofuran

1 INTRODUCTION

Osteoporosis is a systemic disease in which the rigidity and mechanical stability of bones decrease. Bone health in an adult involves the continual removal of old or damaged bone tissue by osteoclasts (OCs) through a process called resorption, which is balanced by the equivalent deposition of new bone by osteoblasts (OBs).^(1,2) As the skeleton ages, the action of OCs outpaces that of OBs, leading to a shift toward excess resorption and development of the chronic degenerative condition osteoporosis; this reduces bone mineral density (BMD) and increases the risk of bone fractures.^(3,4) Osteoporosis has classically been divided into primary (postmenopausal women and people over 70 years old), secondary (caused at least in part by other diseases or therapies), and idiopathic forms.^(4,5) The most common forms of primary osteoporosis occur as a result of menopause and aging. Secondary osteoporosis can result from, for example, the chronic use of glucocorticoids and other drugs, systemic diseases, endocrine diseases, and malignant neoplasms.⁽⁶⁻⁸⁾ Currently, it is estimated that over 200 million people worldwide suffer from this disease, and osteoporosis is the cause of more than 8.9 million fractures annually.^(9,10) Although osteoporosis typically occurs in women, it is also diagnosed in men, who account for an estimated one in five Americans with osteoporosis or low BMD.⁽¹¹⁾ In 2015, direct medical costs totaled \$637.5 million for fatal fall injuries and \$31.3 billion for nonfatal fall injuries. During that same year, hospitalizations for falls cost an average of \$30,550 per admission, totaling \$17.8 billion.⁽¹²⁾ By 2025, the cost of fractures in the United States is

expected to exceed \$25 billion per year for the treatment of more than three million fractures. In addition to being the major cause of fractures in elderly individuals, osteoporosis is highly associated with the occurrence of becoming bedridden, which can lead to serious complications.⁽¹³⁾

Understanding how osteoporosis develops and how to treat it has important socioeconomic and medical consequences. Efforts have primarily concentrated on the development of drugs that block bone resorption by decreasing the differentiation and activity of OCs or on the development of drugs that promote bone formation by increasing the differentiation and activity of OBs. The first category encompasses the antiresorptive agents, which are the most commonly prescribed osteoporosis medications, and include nitrogen-containing bisphosphonates, denosumab, raloxifene, hormone replacement therapy, and calcitonin.⁽¹⁴⁾ By inhibiting OC bone resorption, these therapies are able to improve the quality of life of patients with osteoporosis. However, they cannot restore the skeletal integrity in most patients with established osteoporosis, and they have various side effects.⁽¹⁵⁻²⁵⁾ Recently, attention has turned to the second category mentioned above, the bone anabolic agents. Such agents have the ability to increase bone mass and strength, potentially reversing the structural damage. To date, only one bone anabolic drug is available on the market. The discovery of more novel, cost-effective bone anabolic agents is therefore a priority to treat those suffering from this debilitating condition. Such agents will provide an additional option for osteoporosis patients and

represent a major advancement in the treatment of osteoporosis.

Anabolic therapies that stimulate bone formation are ideal therapies for patients with osteoporosis. Despite the promise of various proteins (e.g., bone morphogenetic protein-2 (BMP-2)) as anabolic agents to increase bone formation, many are not optimal for therapeutic applications due to their side effects outside the skeletal system and their long protein sequences, which result in high manufacturing costs, limited supplies, and susceptibility to enzymatic degradation.⁽²⁶⁻²⁷⁾ Thus, there is a need for inexpensive, novel agents that promote bone formation to effectively treat bone loss. The selective augmentation of BMP-2 in OBs by small molecules that are orally effective may be considered a advancement in this field.

Our research team has established a screening model for the BMP-2 protein. In this screening, we found that 1-(benzo[b]thiophen-2-yl)ethanone (**1**) could upregulate the expression of BMP-2.⁽²⁸⁾ Therefore, derivatives of **1** were synthesized, and their ability to upregulate BMP-2 was evaluated *in vitro*. Based on these results, SAR studies was performed to guide the next-step synthesis studies. Three cycles of structural optimization were performed based on the precursor.⁽²⁹⁻³²⁾ The SAR data revealed that the C-3 methyl group in the benzothiophene or benzofuran moiety did not enhance BMP-2 expression,⁽²⁹⁾ the methyl carboxylate-substituted C-5 phenyl ring may be beneficial to enhance BMP-2 expression,⁽³⁰⁻³²⁾ the C-6 position is more favorable for substitution than the other positions, and the 2-carboxylate group is very important for the potent effects of the 1-(benzo-[b]thiophen/furan-2-yl) thanone analogs.⁽³²⁾ (Figure 1) A

few derivatives of precursor **1** with higher activity were identified. Derivative **8a** showed the highest activity in the senescence-accelerated mouse prone 6 (SAMP-6) model,⁽³⁰⁾ while **38** showed the highest activity in a glucocorticoid-induced osteoporosis model, with similar therapeutic effects to those of raloxifene. The safety of **38** was also systematically evaluated in rat models, and the results indicated that **38** was safe, exhibiting low toxicity and making it worthy of further study.⁽³²⁾

Preliminary pharmacokinetic experiments suggested that there was high lipophilicity and poor metabolic stability of both **38** and **8a**. The prototype drugs were undetectable within 2 minutes in liver microsomes and within 5 minutes in plasma. To improve their therapeutic effects *in vivo*, the ester chain of **38** and **8a** was either extended or substituted with a long-chain amide, and the side-chain proton donor was salified to improve the metabolic stability and hydrophilicity. 20 derivatives which were not reported in the literature were designed and synthesized in this work. An ovariectomized (OVX) rat model of osteoporosis was selected to evaluate the therapeutic effects of the synthetic compounds toward estrogen deficiency-induced osteoporosis. A study was also conducted using a zebrafish osteoporosis model, and the early ADME parameters of the compounds were evaluated.

2 RESULTS AND DISCUSSION

2.1 Chemistry

Although drugs with strong lipophilicity possess better membrane permeability, their high lipophilicity also results in high metabolic clearance rates and strong first-pass effects, leading to poor stability. In addition, drugs possessing low solubility have limited absorption into the blood and circulatory system due to their low solubility in the aqueous phase, and most would be excreted in the feces.⁽³³⁾ Therefore, we had to improve the absorption and stability of the oral medications by balancing their lipophilicity and hydrophilicity to improve their pharmaceutical efficacy.

To improve the metabolic stability and hydrophilicity of compounds **38** and **8a**, we designed 12 substituted benzofuran analogs and 8 substituted benzothiophene analogs. The synthesis of these 20 analogs is shown in Scheme 1. The desired compounds (**114–125**, **132–139**) with different C-2 substituents as well as diverse substituents on the phenyl ring were synthesized using **38**, **8a**, and **38a** as the starting materials. Intermediates **112**, **128**, and **129** were obtained through the reaction of **38**, **8a**, and **38a** with dioxane, respectively, in 0.1 N sodium hydroxide at 40 °C. The reactions of **112**, **128**, and **129** with thionyl chloride in the presence of dimethyl formamide generated the corresponding targets **113**, **130**, and **131**, respectively. Compounds **113**, **130** and **131** were then reacted with a substituted alcohol or amine in the presence of triethylamine in anhydrous toluene to afford the desired products (**114–118**, **123**, **124**, **132–136**, and **139**). The salinization of **115**, **123**, **134**, and **135** by methanesulfonic acid in ethyl alcohol produced the desired compounds **119**, **125**, **137**, and **138**, respectively. Title compounds

120 and **121** were synthesized by first replacing the phosphate ethyl ester group with a trimethylsilyl group, followed by alkaline hydrolysis to remove the siloxy group of **117** and **118**, respectively, in the presence of bromotrimethylsilane. The desired product **122** was obtained through the reaction of **120** with sodium hydroxide.

2.2 *In vitro* evaluation of hydrophilicity

The solubilities of the derivatives of precursors **38** and **8a** were evaluated by precipitation after dilution in PBS solution (PBS containing 0.05% Tween-20, pH=7.4). A total of 16 compounds were dissolved in DMSO with 2-fold serial dilutions, and these DMSO serial solutions were further diluted 10-fold in the PBS solution. The samples precipitated to varying degrees after PBS dilution (marked as “+” for precipitation). The results showed that the hydrophilicity of the derivatives was greatly improved compared with that of the precursors **38** and **8a**. As shown in Table 1, derivative **120** did not precipitate even at the highest tested concentration and showed the best hydrophilicity; derivatives **114**, **115**, **116**, **121**, **123**, **124**, **133**, and **134** also showed better hydrophilicity than **38** and **8a**.

Table 1. Precipitation of the derivatives in the PBS dilution*.

| Compound | Concentration (nM) | | | | | | |
|------------|--------------------|------|------|------|-----|-------|--------|
| | 10000 | 5000 | 2500 | 1250 | 625 | 312.5 | 156.25 |
| 114 | ++ | - | / | / | / | / | / |
| 115 | ++ | - | / | / | / | / | / |
| 116 | ++ | - | / | / | / | / | / |
| 120 | - | / | / | / | / | / | / |
| 121 | ++ | - | / | / | / | / | / |
| 123 | ++ | + | - | / | / | / | / |
| 124 | ++ | ++ | - | / | / | / | / |
| 132 | ++ | ++ | + | + | - | / | / |
| 133 | ++ | ++ | + | - | / | / | / |
| 134 | ++ | ++ | + | - | / | / | / |
| 135 | ++ | ++ | + | + | - | / | / |
| 136 | ++ | ++ | ++ | ++ | + | - | / |
| 139 | ++ | ++ | ++ | + | - | / | / |
| 8a | ++ | ++ | ++ | ++ | ++ | + | - |
| 38 | ++ | ++ | ++ | + | - | / | / |
| 38a | ++ | ++ | ++ | ++ | ++ | + | + |

*"/" No solids are precipitated and the solution is clear; "+" Solids are precipitated sporadically and some of them are visible in the solution; "++" Large number of solids are precipitated and the solution is turbid.

We then selected compounds for *in vivo* experiments. Compound **120**, with the best hydrophilicity in the PBS assay, was selected as the first choice. Then, to compare the SAR and to investigate the influences of different terminal substituents on the activity, **115**, with the same carbon backbone as **120**, was chosen from the group of **114**, **115**, and **116**. To compare the influences of ester and amide derivatives on the *in vivo* activity, compound **123**, the amide derivative with the highest hydrophilicity, was selected. In addition, to compare the influences of sulfur and oxygen atoms on the *in vivo* activity, **135**, the sulfur-containing derivative of precursor

38, was selected for the *in vivo* experiments. For the derivatives of **8a**, compound **134**, with a cyclic aliphatic hydrocarbon side chain, was selected among the compounds with similar hydrophilicity for the *in vivo* experiments. The polarity and water solubility of the 5 chosen derivatives could be improved after salification. Therefore, **115**, **123**, **134**, and **135** were salified to their corresponding methanesulfonic acid derivatives **119**, **125**, **137**, and **138**, while **120** was salified to its disodium salt derivative **122** (Figure 2).

2.3 Activity screening assays in OVX-induced osteoporosis rats and preliminary SAR studies

In previous studies,^(29–32) the bioactivity of precursor **1** and its derivatives were evaluated in senile osteoporosis mouse models (SAMP-6) and drug-induced osteoporosis models (glucocorticoid-induced osteoporosis in rats). Compounds **38** and **8a**, with excellent activity, were identified as the precursors for the current study. In the current study, the OVX rat model of osteoporosis was selected to evaluate the therapeutic effects of the derivatives on estrogen deficiency-induced osteoporosis and summarize the overall treatment effect of such structures on the three types of osteoporosis.

First, the preliminary acute toxicity in Kunming mice was assessed. Compounds **119**, **122**, **125**, **137**, and **138** were all given to the mice orally at a dosages of 500 mg/kg/day for 3 days, and the animals were closely monitored during the first 3 days and the following 14 days. No animals died during the 17 days of observation, indicating that the LD₅₀ values of all compounds

were greater than 500 mg/kg po.

2.3.1 Influences of the elected compounds on the morphology of tibia tissue in OVX-induced osteoporosis rats

Figure 3A shows stained slices of trabecular bone tissue from all groups of OVX-induced osteoporosis rats. The number of trabeculae increased in the groups treated with **1**, **38**, **119**, **125**, and raloxifene compared with that in the untreated model group, with increased thickness and narrowed gaps between the trabeculae in the treatment groups, suggesting positive therapeutic effects in OVX-induced osteoporosis rats.

2.3.2 Effects of the tested compounds on trabecular bone volume (TBV%) of tibia and BMD of L4-6 in OVX-induced osteoporosis rats

As shown in Figure 3B–D, the TBV% and BMD of the untreated model rats significantly decreased compared with that of the blank control (MC) group and the sham group, while no significant difference was observed between the MC group and the sham group. Therefore, the influence of the surgery alone on the results was excluded, and the establishment of the animal model was successful. Compared with the mice in the untreated model group, the TBV% and BMD of the seven test groups and the raloxifene group significantly increased, indicating positive therapeutic effects. The TBV% and BMD of the mice treated with **125** and **119** were

higher than those of in precursor **38** group. The optimal derivative **125** was less effective than the positive control raloxifene.

In summary, derivatives **119** and **125** had similar or stronger activity than precursor **38**, suggesting that improved hydrophilicity could improve the therapeutic effects. Due to limited resources, only 7 compound groups were evaluated, and the preliminary SAR comparisons among these compounds suggested that the derivatives of **38** presented higher bioactivity than the derivatives of **8a** and **38a**. Therefore, precursor **38** was a better structural parent compound for further modification. The activity of compound **125** was higher than that of **119**, indicating that the activity of the amide side chains may be better than the activity of the ester side chains. Therefore, in future studies, more derivatives with amide side chains will be considered when designing experiments.

2.4 Evaluation of the activity and mechanism of action of anti-osteoporotic compound 125 in a zebrafish model

During preliminary studies, we found that anti-osteoporosis activity experiments in mammals required an extended experimental period, complex technologies, and high research costs, which became a technical bottleneck in the research and development of new anti-osteoporosis drugs. Zebrafish belong to the group of “lower vertebrates” and feature a small size and intact bones. The key genes involved in the regulation of bone formation (e.g.,

runx2-related transcription factor 2 (Runx2) and osteonectin) are highly homologous with their mammalian counterparts.⁽³⁴⁾ To overcome the problems listed above, our institute established a zebrafish-based osteoporosis model, which dramatically shortened the experimental period and enhanced research efficiency compared with that of the mammalian models. Moreover, the new model overcomes the shortcomings of experiments that use osteoblast and osteoclast cell models outside the body, such as the strict experimental conditions, the single section where the experiments are applicable and that the experiment results could hardly reflect the internal comprehensive effects. The dexamethasone zebrafish model was used to evaluate lead compound **1**, and we found that the result was highly consistent with that of the rat model.⁽³⁵⁾ Therefore, we adopted the zebrafish model to assess the anti-osteoporotic activity of compound **125**. Concurrently, we used this model to study the anti-osteoporosis mechanism of action.

2.4.1 Activity evaluation using the dexamethasone zebrafish osteoporosis model

The experimental results from the dexamethasone zebrafish osteoporosis model are shown in Figure 4A. The stained area in the dexamethasone-treated zebrafish was apparently smaller than that in the untreated fish, indicating that dexamethasone can significantly lower the degree of bone mineralization in the zebrafish and that the model was established successfully. The results show that compared with the model group, the stained area of the bone in the groups treated with 1, 5, and 25 μM **125** was significantly increased. Image-Pro Plus 6.0 software was

used to analyze the branchial bones on the left flank of the embryos and calculate the total stained area of the branchial cleithrum, branchial compass, branchial abopercular, and branchiostegal rays as well as the total value of the integrated optical density (IOD). With the control group of the untreated fish (MC) considered to have a value of 1.00, the results of all groups, presented as fractions, are shown in Figure 4B and C. The findings reveal that treatment with compound **125** at all concentrations could improve the stained bone area of the zebrafish and the optical density of the stained bone compared with that of the model group, suggesting that **125** could alleviate the bone loss induced by dexamethasone. This improvement was dose-dependent. Treatment with 25 μM **125** could offset most of the bone mineralization damage caused by dexamethasone, bringing the degree of bone mineralization close to normal.

*2.4.2 Influence of **125** on BMP-2 expression in the zebrafish osteoporosis model*

Protein extracts of the untreated control (MC) zebrafish, dexamethasone-treated (model) zebrafish, and zebrafish treated with 1 μM **125** for 24 h were prepared. Western blots were used to show the relative expression levels of BMP-2. The results revealed that the relative expression levels of the BMP-2 protein in the model group was dramatically lower than that of the MC group, indicating that dexamethasone treatment can lower the expression level of BMP-2 (Figure 4D and E). In contrast, the expression level of BMP-2 in the group treated with **125** was

significantly higher than that of the model group and approached the level in the MC group. This indicates that **125** can ameliorate the expression of the BMP-2 protein.

2.4.3 Effect of **125** on Runx2 transcription *in vitro*

Runx2 is a key transcription factor in osteoblast differentiation. Compounds that effectively activate Runx2-driven transcription can induce osteoblast differentiation. After confirming that **125** could upregulate the BMP-2 protein, we further investigated whether **125** could upregulate Runx2 transcription. MC3TC cells were transiently transfected with the plasmid p6OSE2-luc and treated with the tested compounds for 48 h. Then, the activity of the firefly luciferase reporter was measured to investigate the effects of the compounds on Runx2 transcription. Compound **125** was tested in this assay, with lovastatin as the positive control. The results show that the upregulation induced by 10 μM lovastatin was as high as 255.6% of the untreated cell level, but 100 μM lovastatin was apparently cytotoxic. Compound **125** had the highest efficacy at 100 μM , upregulating luciferase activity to 267.2%, which was even higher than the upregulation obtained with lovastatin at the optimal dosage (Figure 4F). These results indicate that **125** could effectively activate Runx2 transcription and could have inductive effects on osteoblast differentiation.

Considering the results of the above three experiments, by enhancing the expression of the BMP-2 protein, **125** may effectively activate Runx2-driven transcription, which could further induce osteoblast differentiation and improve the bone mass of the zebrafish.

2.5 Study on the early ADME properties of active compounds

After determining the anti-osteoporosis activity of compounds of this type through *in vivo* tests, we initiated ADME research to examine the pharmacological performance of these compounds as drugs.

2.5.1 Unidirectional permeability of the test compounds in Caco-2 cells

As a tool for the rapid screening of drug absorption capacity, the Caco-2 test was deemed key in the early screening of oral medications. The apparent permeability coefficient (Papp) obtained from Caco-2 cells correlates well with human intestinal absorption.⁽³⁶⁾ After preparation of the Caco-2 cells, we measured the value of the apical to basolateral transepithelial electrical resistance (TEER AP-BL) and lucifer yellow (LY) leakage AP-BL to evaluate monolayer integrity, during which we also verified the accuracy of the model by introducing metoprolol, erythromycin, and cimetidine as control compounds. As shown in Table 2, the results of the Papp (AP-BL) measurements of **1**, **38**, and **125** indicate relatively good intestinal absorption of **1** and

125 but poor absorption of the lead compound **38**. The Papp value of **125** was higher than that of **38**.

Table 2. Permeability results of the test compounds in the Caco-2 cell line.

| Compound | Papp (AP-BL) ($\times 10^{-6}$, cm/s) | TEER AP-BL ($\Omega \times \text{cm}^2$) | LY Leakage AP-BL (%) |
|---------------------|--|---|-------------------------|
| Metoprolol | 32.6 | 326 | 0.154 |
| Erythromycin | 0.0324 | 396 | 0.137 |
| Cimetidine | 0.679 | 318 | 0.134 |
| 1 | 22.1 | 351 | 0.179 |
| 38 | < 0.00247* | 373 | 0.152 |
| 125 | 9.34 | 341 | 0.158 |

* Receiver sample AB was below the limit of quantification (BLOQ).

2.5.2 Metabolic stability of the test compounds in pooled human liver microsomes

We then used human liver microsomes for the metabolic stability study to evaluate the metabolism and clearance rate of the compounds *in vitro*. We verified the accuracy of the model with phenacetin, verapamil, metoprolol, imipramine, benzydamine, and diclofenac. As shown in Table 3, the evaluation of **1**, **38**, and **125** revealed short half-lives for the *in vitro* metabolism of **1** and **38**, as well as large intrinsic clearance rates and poor metabolic stability. In contrast, the half-life for the *in vitro* metabolism of **125** was significantly longer than that of lead compound **38**, with a smaller intrinsic clearance rate and better metabolic stability (Table 3).

Comprehensively considering the two tests, the ADME properties of **125** were significantly

better than those of the lead compound, which was consistent with the original goal of the current round of derivative design.

Table 3 Metabolic stability of the test compounds in pooled human liver microsomes.

| Compound | <i>In vitro</i> $t_{1/2}$ (min) | CL_{int} ($\mu\text{L}/\text{min}/\text{mg}$ protein) |
|--------------------|---------------------------------|--|
| Phenacetin | 26.5 | 26.2 |
| Verapamil | 3.40 | 204 |
| Metoprolol | 159.0 | 4.35 |
| Imipramine | 67.0 | 10.3 |
| Benzydamine | 43.1 | 16.1 |
| Diclofenac | 3.52 | 197.0 |
| 1 | 1.25 | >300 |
| 38 | NC* | NC* |
| 125 | 103 | 6.73 |

* *In vitro* $t_{1/2}$ and CL_{int} values could not be calculated. The test compound was only detected at the 0.5 minute time point, which indicates a fast metabolism. CL_{int} , intrinsic clearance

2.5.3 CYP inhibition of the test compounds

We proceeded with the ADME research of **125** to identify whether it could inhibit the hepatic drug-metabolizing enzyme system and thereby affect the efficacy and safety of other drugs. The most important hepatic microsomal enzymes are the CYP450s. We selected the five most common CYP450 enzymes and verified the model with specific inhibitors targeting each of these enzymes. As shown in Table 4, **125** had slight inhibitory effects on CYP2D6 but no inhibitory effects on the other four enzymes; therefore, **125** should have little impact on the metabolism of other drugs.

Table 4. Summary of CYP inhibition results.

| CYP* | 1A2 | 2D6 | 3A4 | 2C9 | 2C19 |
|-----------------------------|------------------------------------|------------------------------------|------------------------------------|------------------------------------|------------------------------------|
| Substrate (μM) | Phenacetin (10) | Dextromethorphan (5) | Midazolam (1) | Diclofenac (10) | Omeprazole (0.5) |
| Inhibitor | Naphthoflavone | Quinidine | Ketoconazole | Sulfaphenazole | Tranlycypromine |
| Compound | IC_{50} (μM) |
| Control | 0.0117 | 0.0356 | 0.0217 | 0.893 | 2.07 |
| 125 | >10 | 7.84 | >10 | >10 | >10 |

* Human liver microsome concentration in the incubation was 0.2 mg/mL, incubation time = 20 minutes

2.5.4 Pharmacokinetic evaluation of the **125** metabolites in Sprague-Dawley rats after *iv* and *po* administration

In the human body, **125** would be hydrolyzed into the acid-form **112** to continue its activity. A simple assessment of the pharmacokinetic parameters of **125** would not accurately represent its *in vivo* pharmacokinetic properties and therapeutic effects. As a result, in the pharmacokinetic rat model, we used *iv* and intragastric administration of the metabolite of **125** and measured its pharmacokinetic parameters. As shown in Table 5, the metabolite of **125** possessed good pharmacokinetic parameters and high oral bioavailability.

Table 5. PK parameters and plasma concentration of the metabolite of **125***.

| | | | | | |
|---------|----------------------------|-----------------|----------|----------------------------|------------------|
| | C_0 (ng/mL) | 17.2 ± 3.46 | | $T_{1/2}$ (h) | 4.53 ± 0.28 |
| | $T_{1/2}$ (h) | 2.52 ± 0.89 | | T_{max} (h) | 0.50 ± 0.00 |
| iv | AUC_{0-t} (ng·h/mL) | 59.5 ± 24.7 | po | C_{max} (ng/mL) | 54.2 ± 16.2 |
| 2 mg/kg | $AUC_{0-\infty}$ (ng·h/mL) | 69.0 ± 21.6 | 10 mg/kg | AUC_{0-t} (ng·h/mL) | 278.0 ± 28.0 |
| | MRT (h) | 2.85 ± 0.31 | | $AUC_{0-\infty}$ (ng·h/mL) | 286.0 ± 30.0 |
| | | | | Bioavailability (%) | 83.1% |

* means \pm SD, n=3, except for Bioavailability

2.6 BALB/C mice 14-Day toxicology study

This experiment aimed to evaluate the *in vivo* toxic responses to **38** and **125**. BALB/C mice were divided into a control group, the **38** (100 mg/kg) group, the **38** (50 mg/kg) group, the **125** (100 mg/kg) group and the **125** (50 mg/kg) group to observe the status and growth of the BALB/C mice and evaluate the influence of the compounds on the 14 days following intragastric administration. Indicators of observation included hair, behavioral changes and neurological signs (fremitus, convulsion, spasm, gait disturbance, etc.). After 14 days, all mice were weighed and then dissected to observe the pathological changes in their organs; routine blood tests and blood biochemistry analyses were also performed to study the relationship between the dose and the toxic responses in mice and the extent of damage to the main target organs. The experiment

also explored the tolerant dose range in laboratory animals and the safe dose range that was free of any toxic response.

According to the results of the toxicity study, the mice in the 4 medication administration groups and the control group gained weight well, with no significant difference among the groups. In the 4 medication administration groups, the hair of the animals was glossy and no significant behavioral changes or neurotoxic symptoms were found. Some of the liver biopsies showed a minor degree of hepatocyte nucleus mitosis, megakaryocyte and inflammatory infiltration, and hepatocyte necrotic foci, etc., with no significant difference among the different groups. Some renal biopsies indicated necrosis in individual renal tubular epithelial cells to a minor degree instead of necrosis on the whole, but no significant difference among the groups was found. During the treatment course, no tissue damage was observed in the livers or kidneys of mice treated with 38 and 125 (Figure 5A). Additionally, the serum ALT, aspartate transaminase (AST), urea, and Cre levels of the mice treated with 38 and 125 were still in the normal range (Figure 5B-E).

3 CONCLUSIONS

In this study, the ester chains of precursors **38** and **8a** were extended or substituted with a long-chain amide, and the side-chain proton donor was salified to improve metabolic stability and hydrophilicity. We desired to improve the pharmacokinetic properties of **38** and **8a**, which

we had previously established as having excellent anti-osteoporosis activities. A total of 20 derivatives were designed and synthesized, none of which had been previously reported in the literature, and all showed improved hydrophilicity compared with that of the precursor.

Five compounds with the highest hydrophilicity were selected for evaluation in an OVX-induced osteoporosis rat model. The TBV% and BMD of the groups treated with **119**, **125**, **38**, and **1** were higher than those of the untreated model group but lower than those of the raloxifene group. Compound **125** demonstrated better properties than those of its precursor **38**. This indicated that the goal of improving the *in vivo* therapeutic efficacy of the precursor compound by improving the pharmacokinetic properties was achieved. Preliminary SAR comparisons among these compounds suggested that precursor **38** was a better structural parent compound than **8a** and that amide side chains could produce better activity than lipid side chains.

Our institute established a zebrafish model of hormone-induced osteoporosis. With this model, the therapeutic effects of test drugs can be evaluated within 2 weeks using a simplified operation; thus, *in vivo* activity screening in batches is possible. All of these factors provide a solid foundation for the more rapid and accurate identification of novel anti-osteoporosis drugs. This study verified the anti-osteoporosis activity of **125** with the zebrafish osteoporosis model, and we further quantitatively evaluated BMP-2 protein expression in zebrafish. The results showed that **125** could effectively enhance BMP-2 protein expression. Runx2 is a key transcription factor in OB differentiation. We found that **125** could effectively activate

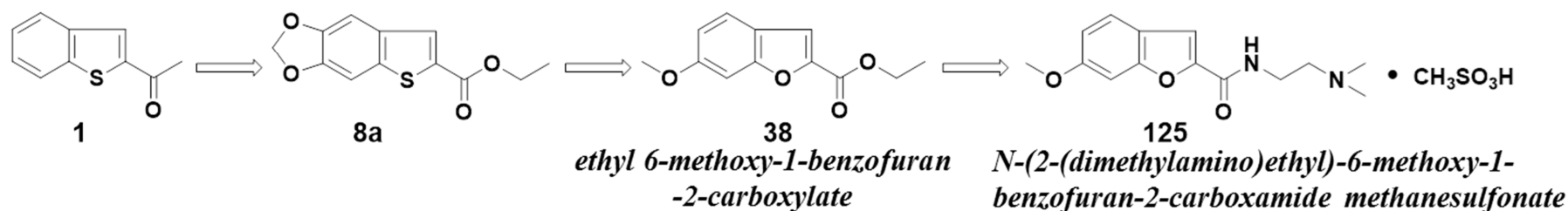
Runx2-driven transcription. These results confirmed the mechanism of how these compounds enhance OB activity and protect against osteoporosis. In addition, this model could be used for future *in vitro* verification of compounds that upregulate BMP-2.

After verifying the anti-osteoporosis activity of **125**, we evaluated its early ADME properties. In both the Caco-2 cell absorption and liver microsome stability tests, compound **125** presented better parameters than those of compounds **38** and **1**. These results are in agreement with the original goal of the current round of derivative design, which was to significantly enhance the absorptive capacity and stability of **125** compared with that of the lead compound **38**. We also learned from the CYP450 enzyme inhibition test that **125** should have little impact on the metabolism of other drugs, which reflects its safety. The metabolite of **125** showed good pharmacokinetic parameters and high oral bioavailability. Moreover, the high likelihood of oral administration of **125** is of great importance to osteoporosis patients in need of chronic drug administration.

Based on BMP-2 screening, our group first discovered that lead compound **1**, which had a novel structure, possessed anti-osteoporosis activity, and we completed three rounds of structural optimization of **1** over the years. During this process, our group synthesized more than 150 new compounds. Moreover, our group created multiple evaluation models related to osteoporosis at both the cellular and animal level and thereby noticeably improved the level of the research platform. Representative compound structures and major experimental results are

shown in Table 6.

Journal Pre-proof

Table 6. Major experimental results on these compounds of our group.

| Experimental content | Compound | | | | |
|---|----------------------------------|--|----------------------------------|---|------------------------------|
| | 1 | 8a | 38 | 125 | Positive control |
| Upregulated activity of BMP-2 expression <i>in vitro</i> ^a _b | Upregulated 35.6% | Upregulated 64.2% | Upregulated 89.4% | Not Done | Lovastatin Upregulated 20.9% |
| Effects on bone histomorphometry in SAMP6 mice ^a | Lower than the positive control | Slightly lower than the positive control | Not Done | Not Done | Lovastatin |
| Effects on bone histomorphometry in glucocorticoid-induced osteoporosis rats ^b | Higher than the positive control | Lower than the positive control | Higher than the positive control | Not Done | Alfacalcidol |
| Effects on bone histomorphometry in OVX-induced osteoporosis rats ^c | Lower than the positive control | Not Done | Lower than the positive control | Lower than the positive control, higher than 1 and 38 | Raloxifene |
| Effects on bone histomorphometry in zebrafish-based osteoporosis | Not Done | Not Done | Not Done | Offset most of the bone mineralization | Not Done |

| | model ^c | | | | damage | |
|-----------|---|--|---|--|--|---|
| Toxicity | Preliminary acute toxicity in Kunming mice ^{a, b, c} | 5000 mg/kg/day orally, 3 days No animals died | 500 mg/kg/day orally, 3 days No animals died | 500 mg/kg/day orally, 3 days No animals died | 500 mg/kg/day orally, 3 days No animals died | Not Done |
| | Pathological sections of the hearts, livers, spleens, lungs, and kidneys of rats ^a | 150 mg/kg/day orally, 3 months No pathological changes | Not Done | Not Done | Not Done | Not Done |
| | Pathological sections of the hearts, livers, spleens, lungs, and kidneys of SAMP6 mice ^a | 30 mg/kg/day orally, 3 months No pathological changes | 30 mg/kg/day orally, 3 months No pathological changes | Not Done | Not Done | Not Done |
| | Blood hematology and biochemistry of rats with glucocorticoid-induced osteoporosis ^b | 30 mg/kg/day orally, 3 months No effects | 30 mg/kg/day orally, 3 months No effects | 30 mg/kg/day orally, 3 months No effects | Not Done | Alfacalcidol 30 mg/kg/day orally, 3 months No effects |
| | BALB/C mice 14-Day toxicology tests ^c | Not Done | Not Done | 100 mg/kg/day orally, 14 days No effects | 100 mg/kg/day orally, 14 days No effects | Not Done |
| Mechanism | Immunohistochemical analysis of BMP-2 expression in the femora of SAMP6 mice ^a | Increased BMP-2 expression | Increased BMP-2 expression | Not Done | Not Done | Lovastatin |
| | The influence on the BMP-2 expression of the zebrafish-based osteoporosis model ^c | Not Done | Not Done | Not Done | Enhanced the expression of the BMP-2 protein | Not Done |

| | | | | | | |
|--|---|----------|----------|----------|---|------------|
| | Effect on Runx2 transcription <i>in vitro</i> ^c | Not Done | Not Done | Not Done | Effectively activated transcription | Lovastatin |
|--|---|----------|----------|----------|---|------------|

^a Our group published in The Journal of Medicinal Chemistry in 2010.⁽³⁰⁾

^b Our group published in The European Journal of Medicinal Chemistry in 2015.⁽³²⁾

^c Content of this article

Journal Pre-proof

In terms of activity, through two rounds of SAR studies, the anti-osteoporosis activity of each round of derivatives was better than that of the previous round. Among these derivatives, **38** showed therapeutic effects in the glucocorticoid rat model that were better than those of the positive control drug, leading to almost normalized values. During the third round of structural modification, both the therapeutic effects and pharmacological performance of the compounds were enhanced by improving their pharmacokinetic properties. Three large-scale animal tests were adopted, each representing a different type of osteoporosis for a more thorough evaluation of the therapeutic effects of these compounds. The results indicated that compounds of this type worked well on senile osteoporosis (SAMP-6 mouse model) and drug-induced osteoporosis (glucocorticoid rat model) but did not work well on osteoporosis resulting from menopause (OVX rat model).

We assessed the safety of these compounds by evaluating the overall state of the animals and the visceral and blood indexes; the results indicated low toxicity. A preclinical study on the toxicity of **125** will be started shortly.

Regarding the mechanism of action of the compounds, using cellular, zebrafish, and mouse models, we verified that these compounds exhibited their anti-osteoporosis effects via osteogenesis and upregulation of BMP-2. As a result, these compounds could correct bone loss that is already occurring in patients, which is difficult for the existing first-tier drugs currently in clinical practice. In addition, these new compounds could be used in combination with existing

clinical drugs to achieve better therapeutic efficacy.

In summary, this paper proposed the optimization of the structure of compound **38** by balancing its lipophilicity and improving its stability, from which we obtained compound **125** with significantly enhanced ADME properties, improved therapeutic efficacy, and better drug performance. Additionally, we completed an evaluation of the anti-osteoporosis effects of the compounds of this type, preliminarily determined the target patient population, verified the mechanism, clarified the level of toxicity, provided a preliminary ADME study, and established a direction for future experimentation. We believe these compounds are of broad clinical applicability, and we will conduct future in-depth studies on them.

4 EXPERIMENTAL SECTION

4.1 Synthesis and characterization

The ^1H NMR and ^{13}C NMR spectra were recorded using TMS as the internal standard in DMSO- d_6 or CDCl_3 with a Bruker BioSpin GmbH spectrometer at 400, 500 and 600 MHz, respectively. The mass spectra (MS) were recorded on a Thermo Scientific LTQ ORBITRAP instrument with an ESI mass selective detector. Melting point (m.p.) values were determined using an SRS-OptiMelt automated melting point instrument without correction. Flash column chromatography was performed with silica gel (200-300 mesh) purchased from Qingdao Haiyang Chemical Co. Ltd.

4.1.1 6-Methoxybenzofuran-2-carboxylic acid (**112**)⁽³⁷⁾

Compound **38** (1.1 g, 5 mmol) was dissolved in 20 mL of dioxane, and 8.0 mL of 1 N NaOH was added. The solution initially became turbid but clarified upon completion of the reaction after 30 minutes. The dioxane was removed by distillation under reduced pressure, and the remaining product was dissolved in water. The solution was mixed with dichloromethane and after stratification, the organic phase was discarded, and the aqueous phase was adjusted to pH=3 with 10% HCl. The precipitate was collected and recrystallized in dry methanol. Finally, 0.51 g (yield of 83%) of solid was obtained. m.p: 195-196°C. ¹H NMR (600 MHz, DMSO-*d*₆) δ (ppm): 3.84 (s, 3H), 6.97 (dd, *J*₁ = 9.0 Hz, *J*₂ = 1.8 Hz, 1H), 7.29 (d, *J* = 1.8 Hz, 1H), 7.59 (s, 1H), 7.64 (d, *J* = 9.0 Hz, 1H), 13.32 (s, 1H).

4.1.2 6-Methoxybenzofuran-2-carbonyl chloride (**113**)

Compound **112** (1.92 g, 0.01 mol) and SOCl₂ (2.8 mL, 0.04 mol) were dissolved in 50 mL of methylbenzene, and 2 drops of DMF were added. The solution was stirred at 80°C with a drying tube attached to the apparatus. Then, the solution was evaporated to dryness under reduced pressure, dissolved in pure methylbenzene and evaporated to dryness again. Product **113** was immediately used for the next reaction.

4.1.3 2-(Dimethylamino)ethyl 6-methoxybenzofuran-2-carboxylate (**115**)

Ten milliliters of pure methylbenzene was added to compound **113** that was generated in the previous step. Triethylamine (2.0 mL, 0.013 mol) and N,N-dimethylethanolamine (1.3 mL, 0.013 mol) were added to the solution with cooling; the reaction was completed at room temperature with stirring within 1 h. Water and ethyl acetate were added to the reaction system, and the aqueous phase was removed after shaking and stratification. The solution was washed twice with water. The organic phase was collected, washed with saturated NaCl solution, and evaporated to dryness. The resulting solid was dissolved in diethyl ether and recrystallized. Finally, 1.90 g of yellow crystals were obtained (yield of 73%). m.p: 38-39°C. ¹H NMR (400 MHz, CDCl₃) δ(ppm): 2.37 (s, 6H), 2.75 (t, *J* = 6.0 Hz, 2H), 3.87 (s, 3H), 4.48 (t, *J* = 6.0 Hz, 2H), 6.93 (dd, *J*₁ = 8.8 Hz, *J*₂ = 2.4 Hz, 1H), 7.06 (d, *J* = 2.0 Hz, 1H), 7.48 (s, 1H), 7.52 (d, *J* = 8.8 Hz, 1H). ¹³C NMR (151 MHz, DMSO-d₆) δ 45.25, 55.72, 57.14, 62.48, 95.84, 114.01, 114.57, 119.27, 123.49, 144.09, 156.60, 158.57, 160.31. HRMS (ESI⁺): found 264.12305[M+H]⁺, (Calcd for C₁₄H₁₈O₄N: 264.12303).

4.1.4 3-(Dimethylamino)propyl 6-methoxybenzofuran-2-carboxylate (**114**)

The title compound was obtained from **113** and 3-(dimethylamino)propan-1-ol (A) using a procedure similar to that used for compound **115**. 1.21 g (yield of 70%) of white solid was obtained. m.p. 71-73°C. ¹H NMR (400 MHz, CDCl₃) δ (ppm): 2.44 (m, 2H), 2.85 (s, 6H),

3.19 (m, 2H), 3.88 (s, 3H), 4.49 (m, 2H), 6.96 (dd, $J_1 = 8.8$ Hz, $J_2 = 2.0$ Hz, 1H), 7.05 (d, $J = 2.0$ Hz, 1H), 7.51 (s, 1H), 7.55 (d, $J = 8.4$ Hz, 1H). HRMS (ESI⁺): found 278.13868 [M+H]⁺, (Calcd for C₁₅H₂₀O₄N: 278.13868).

4.1.5 2-Morpholinoethyl 6-methoxybenzofuran-2-carboxylate (**116**)

The title compound was obtained from **113** and **2-morpholinoethanol** (C) using a procedure similar to that used for compound **115**. 1.03 g (yield of 62%) of white solid was obtained. m.p. 83-84°C. ¹H NMR (400 MHz, CDCl₃) δ (ppm): 2.59 (s, 4H), 2.80 (s, 2H), 3.73 (s, 4H), 3.87 (s, 3H), 4.50 (t, $J = 5.2$ Hz, 2H), 6.94 (dd, $J_1 = 8.8$ Hz, $J_2 = 2.0$ Hz, 1H), 7.06 (d, $J = 1.6$ Hz, 1H), 7.47 (s, 1H), 7.53 (d, $J = 8.8$ Hz, 1H). HRMS (ESI⁺): found 306.13352 [M+H]⁺, (Calcd for C₁₆H₂₀O₅N: 306.13360).

4.1.6 2-(Dimethoxyphosphoryl)ethyl 6-methoxybenzofuran-2-carboxylate (**117**)

The title compound was obtained from **113** and **dimethyl (2-hydroxyethyl)phosphonate** (D) using a procedure similar to that used for compound **115**. Product **117** was immediately used for the next reaction. Yield, 66%; white oil. HRMS (ESI⁺): found 329.07841 [M+H]⁺, (Calcd for C₁₄H₁₈O₇P: 329.07847).

4.1.7 (Diethoxyphosphoryl)methyl 6-methoxybenzofuran-2-carboxylate (**118**)

The title compound was obtained from **113** and **diethyl (hydroxymethyl)phosphonate (E)** using a procedure similar to that used for compound **115**. 0.98 g (yield of 65%) of white oil was obtained. ^1H NMR (400 MHz, CDCl_3) δ (ppm): 1.37 (t, $J = 7.2$ Hz, 6H), 3.88 (s, 3H), 4.20-4.27 (m, 4H), 4.64 (d, $J = 8.4$ Hz, 2H), 6.95 (dd, $J_1 = 8.8$ Hz, $J_2 = 2.0$ Hz, 1H), 7.05 (d, $J = 1.6$ Hz, 1H), 7.59 (d, $J = 8.0$ Hz, 2H). HRMS (ESI $^+$): found 343.09406 [M+H] $^+$, (Calcd for $\text{C}_{15}\text{H}_{20}\text{O}_7\text{P}$: 343.09412).

4.1.8 2-(Dimethylamino)ethyl-6-methoxybenzofuran-2-carboxylate methanesulfonate (**119**)

Compound **115** was dissolved in 10 mL of absolute ethanol, and $\text{CH}_3\text{SO}_3\text{H}$ was added at room temperature. After reacting at 50°C with stirring for 2 h, the solution was cooled in a -18°C freezer to allow crystallization. The crystals were collected, washed with absolute ethanol, and dried. Finally, 0.47 g of white solid was obtained (yield of 86%). m.p: 149-151°C. ^1H NMR (500MHz, CDCl_3) δ (ppm): 2.81 (s, 3H), 3.01 (s, 3H), 3.02 (s, 3H), 3.52 (q, $J = 5.0$ Hz, 2H), 3.88 (s, 3H), 4.78-4.80 (m, 2H), 6.95 (dd, $J = 9.0$ Hz, 2.0 Hz, 1H), 7.03 (d, $J = 2.0$ Hz, 1H), 7.66 (s, 1H), 11.78 (s, 1H). ^{13}C NMR (151 MHz, $\text{DMSO}-d_6$) δ 42.80, 55.13, 55.81, 59.16, 95.85, 114.23, 115.45, 119.66, 123.66, 143.59, 156.76, 158.05, 160.50. HRMS (ESI $^+$): found 264.12302[M- CH_3SO_3] $^+$, (Calcd for $\text{C}_{14}\text{H}_{18}\text{O}_4\text{N}$: 264.12303).

4.1.9 2-((6-Methoxybenzofuran-2-carbonyl)oxy)ethyl)phosphonic acid (**120**)

Compound **117** (1.64 g, 0.005 mol) was dissolved in 10 mL of anhydrous dichloromethane, and trimethylsilyl bromide (4 mL, 0.03 mol) was added at room temperature with stirring for 4 h. Then, 10 mL of anhydrous methanol was added to the solution in an ice bath; the solvent was removed by distillation under reduced pressure, and the remaining solution was adjusted to pH=8 with ammonia water. The precipitated white solid was filtered, washed with methylene chloride, and acidified to pH=2 with 10% HCl. The precipitate was collected and recrystallized from methanol. Finally, 1.14 g of white solid was obtained (yield of 73%). m.p. 153-155°C. $^1\text{H NMR}$ (400 MHz, $\text{DMSO-}d_6$) δ (ppm): 2.06 (dt, $J_1 = 18.8$ Hz, $J_2 = 8.0$ Hz, 2H), 3.83 (s, 3H), 4.44 (dt, $J_1 = 8.8$ Hz, $J_2 = 8.0$ Hz, 2H), 6.98 (d, $J = 8.4$ Hz, 1H), 7.32 (s, 1H), 7.66 (d, $J = 7.2$ Hz, 2H), 10.79 (s, 2H). $^{13}\text{C NMR}$ (151 MHz, $\text{DMSO-}d_6$) δ 28.10, 28.95, 55.68, 62.73, 95.33, 113.74, 115.13, 120.05, 123.55, 143.61, 156.48, 159.91, 160.91. HRMS (ESI⁺): found 323.0290[M+Na]⁺, (Calcd for $\text{C}_{12}\text{H}_{13}\text{NaO}_7\text{P}$: 323.0296).

4.1.10 (((6-Methoxybenzofuran-2-carbonyl)oxy)methyl)phosphonic acid (**121**)

The title compound was obtained from **118** using a procedure similar to that used for compound **120**. 1.17 g (yield of 70%) of white solid was obtained. m.p. 145-146°C. $^1\text{H NMR}$ (400 MHz, $\text{DMSO-}d_6$) δ (ppm): 3.91 (s, 3H), 4.41 (d, $J = 8.4$ Hz, 2H), 7.10 (dd, $J_1 = 8.8$ Hz, $J_2 = 2.4$ Hz, 1H), 7.65 (d, $J = 2.4$ Hz, 1H), 7.94 (d, $J = 8.8$ Hz, 1H), 8.14 (s, 1H). HRMS (ESI⁺): found 309.01441 [M+Na]⁺, (Calcd for $\text{C}_{11}\text{H}_{11}\text{NaO}_7\text{P}$: 309.01401).

4.1.11 Sodium (2-((6-methoxybenzofuran-2-carbonyl)oxy)ethyl)phosphonate (**122**)

To the suspension of compound **120** (1.0 g, 0.0033 mol) in deionized water (10 mL), 0.1 N NaOH (66 mL, 0.0066 mol) was added at room temperature, and the reaction was allowed to proceed for 1 h with stirring. Then, the remaining solution was adjusted to pH=7 with 1 N NaOH. Finally, 0.97 g of white solid was obtained (yield of 85%). m.p.>360°C. ¹H NMR (400 MHz, DMSO-*d*₆) δ(ppm): 1.75-1.83 (m, 2H), 3.83 (s, 3H), 4.37-4.42 (m, 2H), 6.97 (dd, *J*₁ = 8.8 Hz, *J*₂ = 2.0 Hz, 1H), 7.31 (s, 1H), 7.63-7.65 (m, 2H). ¹³C NMR (151 MHz, DMSO-*d*₆) δ 30.98 (d, *J* = 129.6 Hz), 58.66, 65.00, 98.46, 116.78, 118.19, 123.11, 126.60, 146.77, 159.63, 162.98, 163.90. HRMS (ESI⁺): found 345.0108[M+H]⁺, (Calcd for C₁₂H₁₂Na₂O₇P: 345.0116).

4.1.12 *N*-(2-(dimethylamino)ethyl)-6-methoxybenzofuran-2-carboxamide (**123**)

The title compound was obtained from **113** and N¹, N¹-dimethylethane-1,2-diamine (F) using a procedure similar to that used for compound **115**. 1.30 g (yield of 72%) of white oil. ¹H NMR (400 MHz, CDCl₃) δ (ppm): 2.39 (s, 6H), 2.64 (s, 2H), 3.60 (d, *J* = 4.8 Hz, 2H), 3.87 (s, 3H), 6.91 (d, *J* = 8.4 Hz, 1H), 7.03 (s, 1H), 7.26 (s, 1H), 7.40 (s, 1H), 7.53 (d, *J* = 8.4 Hz, 1H). ¹³C NMR (151 MHz, DMSO-*d*₆) δ 34.11, 42.57, 55.72, 55.92, 95.85, 110.05, 113.19, 120.24, 123.14, 147.98, 155.56, 158.83, 159.55. HRMS (ESI⁺): found 263.1390 [M+H]⁺, (Calcd for C₁₄H₁₉O₃N₂: 263.1390).

4.1.13 *N*-(2-(dimethylamino)ethyl)-6-methoxy-*N*-methylbenzofuran-2-carboxamide (**124**)

The title compound was obtained from **113** and *N*¹,*N*¹-dimethyl-*N*²-methyl ethane-1,2-diamine (G) using a procedure similar to that used for compound **115**. 1.33 g (yield of 75%) of white solid. m.p. 33-34°C. ¹H NMR (400 MHz, CDCl₃) δ (ppm): 2.34 (s, 6H), 2.66 (t, *J* = 7.2 Hz, 2H), 3.10-3.37 (m, 3H), 3.74 (s, 2H), 3.85 (s, 3H), 6.91 (dd, *J*₁ = 8.8 Hz, *J*₂ = 2.0 Hz, 1H), 6.99 (s, 1H), 7.29 (s, 1H), 7.49 (d, *J* = 8.4 Hz, 1H). HRMS (ESI⁺): found 277.15461 [M+H]⁺, (Calcd for C₁₅H₂₁O₃N₂: 277.15467).

4.1.14 *N*-(2-(dimethylamino)ethyl)-6-methoxybenzofuran-2-carboxamide methanesulfonate (**125**)

The title compound was obtained from **123** using a procedure similar to that used for compound **119**. 1.38 g (yield of 82%) of white solid was obtained. m.p. 117-120°C. ¹H NMR (400 MHz, DMSO-*d*₆) δ (ppm): 2.30 (s, 3H), 2.85 (s, 6H), 3.27 (d, *J* = 4.4 Hz, 2H), 3.59-3.63 (m, 2H), 3.84 (s, 3H), 6.99 (dd, *J*₁ = 8.8 Hz, *J*₂ = 2.0 Hz, 1H), 7.18 (d, *J* = 1.6 Hz, 1H), 7.49 (s, 1H), 7.66 (d, *J* = 8.8 Hz, 1H), 8.78 (t, *J* = 5.6 Hz, 1H), 9.27 (s, 1H). ¹³C NMR (151 MHz, DMSO-*d*₆) δ 34.11, 39.73, 42.56, 55.71, 55.93, 95.84, 110.07, 113.18, 120.23, 123.15, 147.97, 155.55, 158.82, 159.55. HRMS (ESI⁺): found 263.13895 [M-CH₃SO₃]⁺, (Calcd for C₁₄H₁₉O₃N₂: 263.13902).

4.1.15 Thieno[2',3':4,5]benzo[1,2-d][1,3]dioxole-6-carboxylic acid (**128**)

The title compound was obtained from **8a** using a procedure similar to that used for compound **112**. 3.40 g (yield of 83%) of white solid was obtained. ^1H NMR (600 MHz, DMSO- d_6) δ (ppm): 6.12 (s, 2H), 7.42 (s, 1H), 7.54 (s, 1H), 7.90 (s, 1H), 13.19 (s, 1H).

4.1.16 6-Methoxybenzo[*b*]thiophene-2-carboxylic acid (**129**)

The title compound was obtained from **38a** using a procedure similar to that used for compound **112**. 3.51 g (yield of 84%) of white solid was obtained. ^1H NMR (600 MHz, DMSO- d_6) δ (ppm): 3.85 (s, 3H), 7.06 (dd, $J_1 = 9.0$ Hz, $J_2 = 2.4$ Hz, 1H), 7.60 (d, $J = 1.8$ Hz, 1H), 7.88 (d, $J = 8.4$ Hz, 1H), 8.01 (s, 1H), 13.25 (s, 1H).

4.1.17 Thieno[2',3':4,5]benzo[1,2-d][1,3]dioxole-6-carbonyl chloride (**130**)

The title compound was obtained from **128** using a procedure similar to that used for compound **113**. White solid. Product **130** was immediately used for the next reaction.

4.1.18 6-Methoxybenzo[*b*]thiophene-2-carbonyl chloride (**131**)

The title compound was obtained from **129** using a procedure similar to that used for compound **113**. White solid. Product **131** was immediately used for the next reaction.

4.1.19 3-(Dimethylamino)propyl thieno[2',3':4,5]benzo[1,2-d][1,3]dioxole-6-carboxylate (**132**)

The title compound was obtained from **130** and **3-(dimethylamino)propan-1-ol** (A) using a procedure similar to that used for compound **115**. 1.20 g (yield of 73%) of yellow solid was obtained. m.p. 75-77°C. ¹H NMR (400 MHz, CDCl₃) δ (ppm): 1.93-2.00 (m, 2H), 2.30 (s, 6H), 2.48 (t, *J* = 7.2 Hz, 2H), 4.37 (t, *J* = 6.4 Hz, 2H), 6.05 (s, 2H), 7.19 (s, 1H), 7.20 (s, 1H), 7.89 (s, 1H). HRMS (ESI⁺): found 308.09512 [M+H]⁺, (Calcd for C₁₅H₁₈O₄NS: 308.09511).

4.1.20 2-(Dimethylamino)ethyl thieno[2',3':4,5]benzo[1,2-d][1,3]dioxole-6-carboxylate (**133**)

The title compound was obtained from **130** and **2-(dimethylamino)ethan-1-ol** (B) using a procedure similar to that used for compound **115**. 1.13 g (yield of 72%) of yellow solid was obtained. m.p. 90-91°C. ¹H NMR (400 MHz, CDCl₃) δ (ppm): 2.36 (s, 6H), 2.73 (t, *J* = 6.0 Hz, 2H), 4.44 (q, *J* = 6.0 Hz, 2H), 6.05 (s, 2H), 7.19 (s, 1H), 7.20 (s, 1H), 7.90 (s, 1H). HRMS (ESI⁺): found 294.08020 [M+H]⁺, (Calcd for C₁₄H₁₆O₄NS: 294.07946).

4.1.21 2-Morpholinoethyl thieno[2',3':4,5]benzo[1,2-d][1,3]dioxole-6-carboxylate (**134**)

The title compound was obtained from **130** and **2-morpholinoethan-1-ol** (C) using a procedure similar to that used for compound **115**. 0.96 g (yield of 65%) of white solid was obtained. m.p. 131-133°C. ¹H NMR (400 MHz, CDCl₃) δ (ppm): 2.62 (m, 4H), 2.81 (m, 2H), 3.75 (m, 4H), 4.49 (m, 2H), 6.05 (s, 2H), 7.20 (s, 2H), 7.90 (s, 1H). ¹³C NMR (151 MHz,

DMSO- d_6) δ 53.20, 56.25, 62.25, 65.94, 101.72, 101.91, 103.46, 130.53, 130.57, 133.10, 136.41, 147.12, 148.87, 161.72. HRMS (ESI⁺): found 336.08991 [M+H]⁺, (Calcd for C₁₆H₁₈O₅NS: 336.09002).

4.1.22 3-(Dimethylamino)propyl 6-methoxybenzo[b]thiophene-2-carboxylate (**135**)

The title compound was obtained from **131** and **3-(dimethylamino)propan-1-ol** (A) using a procedure similar to that used for compound **115**. 0.88 g (yield of 63%) of white solid was obtained. m.p. 27-28°C. ¹H NMR (400 MHz, CDCl₃) δ (ppm): 1.95 (m, 2H), 2.27 (s, 6H), 2.45 (t, J = 7.2 Hz, 2H), 3.89 (s, 3H), 4.38 (t, J = 6.8 Hz, 2H), 7.01 (dd, J_1 = 8.8 Hz, J_2 = 2.4 Hz, 1H), 7.27 (d, J = 2.4, 1H), 7.73 (d, J = 8.8 Hz, 1H), 7.96 (s, 1H). ¹³C NMR (151 MHz, DMSO- d_6) δ 26.28, 45.04, 55.44, 55.53, 63.45, 104.78, 115.84, 126.64, 130.04, 130.56, 132.37, 143.49, 159.22, 162.04. HRMS (ESI⁺): found 294.11574 [M+H]⁺, (Calcd for C₁₅H₂₀O₃NS: 294.11584).

4.1.23 Butyl 6-methoxybenzo[b]thiophene-2-carboxylate (**136**)

The title compound was obtained from **131** and **butan-1-ol** (H) using a procedure similar to that used for compound **115**. 1.08 g (yield of 67%) of white oil was obtained. ¹H NMR (400 MHz, CDCl₃) δ (ppm): 0.99 (t, J = 7.2 Hz, 3H), 1.46-1.54 (m, 2H), 1.76 (t, J = 6.8 Hz, 2H), 3.89 (s, 3H), 4.34 (t, J = 6.8 Hz, 2H), 7.03 (dd, J_1 = 8.8 Hz, J_2 = 2.4 Hz, 1H), 7.28 (d, J = 2.4 Hz, 1H),

7.73 (d, $J = 8.8$ Hz, 1H), 7.96 (s, 1H). HRMS (ESI⁺): found 265.08935 [M+H]⁺, (Calcd for C₁₄H₁₇O₃S: 265.08929).

4.1.24 2-Morpholinoethyl thieno[2',3':4,5]benzo[1,2-d][1,3]dioxole-6-carboxylate methanesulfonate (137)

The title compound was obtained from **134** using a procedure similar to that used for compound **119**. 1.21 g (yield of 82%) of white solid was obtained. m.p. 208-210°C. ¹H NMR (400 MHz, DMSO-*d*₆) δ (ppm): 2.30 (s, 3H), 3.24 (m, 2H), 3.53-3.72 (m, 8H), 4.00 (m, 2H), 4.63 (m, 2H), 6.15 (s, 2H), 7.49 (s, 1H), 7.63 (s, 1H), 8.10 (s, 1H), 9.82 (s, 1H). ¹³C NMR (151 MHz, DMSO-*d*₆) δ 39.72, 51.65, 54.72, 59.38, 63.31, 101.80, 102.03, 103.50, 129.96, 131.29, 133.10, 136.65, 147.26, 149.08, 161.41. HRMS (ESI⁺): found 336.09000 [M-CH₃SO₃]⁺, (Calcd for C₁₆H₁₈O₅NS: 336.09002).

*4.1.25 3-(Dimethylamino)propyl-6-methoxybenzo[*b*]thiophene-2-carboxylate methanesulfonate (138)*

The title compound was obtained from **135** using a procedure similar to that used for compound **119**. 1.32 g (yield of 88%) of white solid was obtained. m.p. 116-117°C. ¹H NMR (500 MHz, CDCl₃) δ (ppm): 2.31-2.33 (m, 2H), 2.84 (s, 3H), 2.92 (s, 6H), 3.20-3.24 (m, 2H), 3.90 (s, 3H), 4.46 (t, $J = 5.5$ Hz, 2H), 7.05 (dd, $J_1 = 9.0$ Hz, $J_2 = 2.0$ Hz, 1H), 7.28 (d, $J = 2.0$ Hz,

1H), 7.76 (d, $J = 9.0$ Hz, 1H), 8.00 (s, 1H), 11.46 (s, 1H). ^{13}C NMR (151 MHz, DMSO- d_6) δ 23.53, 39.73, 42.34, 53.92, 55.64, 62.28, 104.89, 116.02, 126.76, 129.71, 131.04, 132.36, 143.59, 159.33, 161.97. HRMS (ESI $^+$): found 294.11576 [M-CH $_3$ SO $_3$] $^+$, (Calcd for C $_{15}$ H $_{20}$ O $_3$ NS: 294.11584).

4.1.26 N-(2-(dimethylamino)ethyl)thieno[2',3':4,5]benzo[1,2-d][1,3]dioxole-6- carboxamide
(139)

The title compound was obtained from **130** and **N 1 ,N 1 -dimethylethane-1,2-diamine** (F) using a procedure similar to that used for compound **115**. 1.12 g (yield of 71%) of white solid was obtained. m.p. 150-151°C. ^1H NMR (400 MHz, CDCl $_3$) δ (ppm): 2.37 (s, 6H), 2.62 (t, $J = 6.0$ Hz, 2H), 3.56 (t, $J = 6.0$ Hz, 2H), 6.03 (s, 2H), 6.99 (s, 1H), 7.18 (s, 1H), 7.20 (s, 1H), 7.67 (s, 1H). HRMS (ESI $^+$): found 293.09533 [M+H] $^+$, (Calcd for C $_{14}$ H $_{17}$ O $_3$ N $_2$ S: 293.09544).

4.2 Activity screening assay method in OVX-induced osteoporosis rats

The SD rats were provided by the Experimental Animal Center of the PLA Academy of Military Science. The rats were randomly divided into 3 groups: the blank control group, sham group, and model group. After adaptive feeding for 1 week, the rats in the model group ($n = 10$) received a bilateral ovariectomy, and the rats in the sham group ($n = 10$) received the same surgery except that fat tissue was removed instead of the ovaries. On postoperative day 10, the

model group was further divided into 9 groups ($n = 10$): the untreated model group, raloxifene group, and the seven test groups. The medication groups were then given the corresponding drugs by intragastric gavage (ig): 0.5 mg/mL raloxifene hydrochloride suspension for the raloxifene group with a dosage of 5 mg/kg and 3 mg/mL of the corresponding test drugs for the other 7 groups with a dosage of 30 mg/kg. The drugs were administered QD for 3 months, with a 1-day break after 6 consecutive days of administration. The blank control, sham, and untreated model groups were given equal volumes of pure water via ig administration. All rats were given tetracycline hydrochloride (30 mg/kg) via intraperitoneal injection for fluorescent labeling of the bones 16 days and 3 days before euthanasia. After drug administration, the rats were anesthetized with sodium pentobarbital at a dose of 45 mg/kg, followed by a bone mineral density (BMD) test with an OSTEOCORE 3 Bone Density Meter (Medilink, France). The data were analyzed with the software of the device (V 6.14) for rodent analysis. In the software environment, the bones of the rats were filled manually, and the bone density of such areas was calculated by the software. The bone density images and the processed areas are shown in the front figures.

All animal procedures were performed in accordance with the Guidelines for Care and Use of Laboratory Animals of the Institute of Medicinal Biotechnology, Chinese Academy of Medical Science and Peking Union Medical College and were approved by the Animal Ethics Committee of the Institute of Medicinal Biotechnology.

4.3 Activity screening assay method for the zebrafish model

In groups, zebrafish embryos from AB lines at 6 hpf were incubated in dexamethasone solution for 72 h, and drugs were then administered. Embryos were cultured until 6 dpf and then harvested, followed by alizarin red staining, rehydration, decoloration, photomicrography, and analysis of the staining results. Anti-osteoporosis activity screening experiments were carried out through the above steps in this dexamethasone zebrafish model. The zebrafish were divided into 5 groups. Group A (n = 30) was the model group, and the solution was changed to the zebrafish breeding water. Groups B–D (n = 30) were given different doses of **125**, and the larvae were soaked in the drug solution. Group E (n = 30) was composed of zebrafish that had not been treated with dexamethasone.

We used dexamethasone to induce the zebrafish and establish the osteoporosis model. The experiment consisted of some fish receiving 1 μM **125** while other zebrafish in the normal control group were treated with the fish breeding water. Twenty-four h after we collected the zebrafish the total protein was extracted.

All animal procedures were performed in accordance with the Guidelines for Care and Use of Laboratory Animals of the Institute of Medicinal Biotechnology, Chinese Academy of Medical Science and Peking Union Medical College and were approved by the Animal Ethics Committee of the Institute of Medicinal Biotechnology.

4.4 Assessment of Runx2-driven transcription with the p6OSE2-luc plasmid

Transfection was performed in a 96-well plate. For each well, 100 ng of DNA and 0.4 μ l of TurboFectin 8.0 transfection reagent (OriGene TF81001) was diluted in 10 μ l of serum-free α -MEM medium, and after 5 minutes of incubation at room temperature, the two were mixed and incubated at room temperature for another 20 minutes (the transfection complex was made as a master mix as required). Rapidly growing MC3T3-E1 cells at 90% confluence were digested with trypsin and gently suspended into single cells with α -MEM medium containing 10% FBS, and the cell concentration was adjusted to 10^5 /ml. A total of 100 μ l of single-cell suspensions were added to 20 μ l of the DNA-liposome complex and mixed thoroughly, and this mixture (120 μ l) was added to each well of the 96-well plate. The cells were cultured in a CO₂ incubator at 37°C for 24 h, and then the medium was replaced with 200 μ l of complete medium with the appropriate concentration of the tested compound. The cells were cultured for another 48 h before assessment of luciferase activity with the Luciferase Assay System (Promega E1501).

4.5 Early ADME research methods

4.5.1 Unidirectional permeability in Caco-2 cells

First, the Caco-2 plate was removed from the incubator. Then, the plate was incubated at 37 °C for 30 minutes. A 10 μ M compound working solution was prepared. To determine the rate

of drug transport in the apical to basolateral direction, the plate was incubated at 37 °C for 2 h without shaking. At the end of the transport period, 8 µL of the sample from the donor side was transferred (apical compartment for Ap→Bl flux) into 72 µL of transport buffer and 240 µl of quenching solvent in a new 96-well plate. Similarly, 80 µL of solution was directly removed from the receiver side (basolateral compartment for Ap→Bl flux) and transferred to new 96-well plate with 240 µl of quenching solvent. The samples were vortexed at 1000 rpm for 5 minutes. Then, the samples were centrifuged at 4,000 rpm for 20 minutes. An aliquot of 100 µL of the supernatant mixed with 100 µL of pure water was used for LC/MS/MS analysis. All incubations were performed in duplicate. To the Transwell insert (apical compartment), 100 µL of the Lucifer yellow solution was added and the wells in the receiver plate (basolateral compartment) were filled with 300 µL of transport buffer. After incubation at 37 °C for 30 minutes, 80 µL of solution was directly removed from both the apical and basolateral wells (using the basolateral access holes) and transferred to new 96-well plates. The Lucifer Yellow fluorescence (to monitor monolayer integrity) was measured with a fluorescence plate reader at wavelengths of 485 nm excitation and 530 nm emission.

The apparent permeability coefficient (P_{app}), in units of centimeters per second, can be calculated for the Caco-2 drug transport assays using the following equation:

$$P_{app} = (V_A \times [\text{drug}]_{\text{acceptor}}) / (\text{Area} \times \text{Time} \times [\text{drug}]_{\text{initial,donor}})$$

4.5.2 Metabolic stability in pooled human liver microsomes

First, 1325 μL of a 20 mg/mL HLM solution was added to 22260 μL of phosphate buffer to obtain the HLM mixture at a concentration of 1.1236 mg/mL. Then, 222.5 μL of the HLM mixture and 25 μL of 10 mM NADPH were added to the incubation plates. This solution was mixed on a whirly mixer for 10 seconds. The incubation plate was prewarmed at 37 °C for 8 minutes. The reaction was initiated with the addition of 2.5 μL of the 100 μM test compound solution or PC solution to the incubation plate. Phenacetin, verapamil, metoprolol, imipramine, benzydamine and diclofenac were used in this experiment. This incubation mixture was mixed on a whirly mixer for 12 seconds followed by incubation at 37 °C. The final concentrations of microsomes were 1 mg/mL, and the final concentration of the compounds were 1 $\mu\text{mol/L}$. The reaction was quenched by transferring 20 μL of the incubated mixture after 0.5, 5, 10, 15, 20 or 30 minutes into the quenching plate containing 100 μL of cold stop solution (100 nM alprazolam, 200 nM caffeine and 100 nM tolbutamide). The solution was vortexed at 800 rpm for 2 minutes. Peak areas were determined from the extracted ion chromatograms. The percent parent remaining was calculated from the peak area of the test compound or PC. The slope value, k , was determined by linear regression of the curve of the natural logarithm of the percent parent remaining vs. the incubation time. All calculations were carried out using Microsoft Excel. The *in vitro* half-life (*in vitro* $t_{1/2}$) was determined from the slope value:

$$\textit{in vitro } t_{1/2} = -(0.693/k)$$

Conversion of the *in vitro* $t_{1/2}$ (min) into the *in vitro* intrinsic clearance (*in vitro* CL_{int} , in $\mu\text{L}/\text{min}/\text{mg}$ protein) was performed using the following equation (mean of duplicate determinations):

$$\textit{in vitro} CL_{int} = \frac{0.693}{t_{1/2}} \times \frac{\text{volume of incubation } (\mu\text{L})}{\text{amount of proteins (mg)}}$$

4.5.3 CYP inhibition

An aliquot of 178 μL of the liver microsome working solution with mixed with the substrates in 1.1 mL tubes using a multichannel pipette. For the matrix samples (without the addition of the control inhibitor or test compound), 2 μL of DMSO and 200 μL of quenching solution were added into the tubes, the tubes were vortexed for 1 minute, and then 20 μL of NADPH solution was added. The tubes were capped, vortexed, and placed on ice to wait for the study samples. For the study samples (samples with the added control inhibitor or test compound), 2 μL of the series of control inhibitor stock solutions and the series test compound stock solutions were placed into 1.1 mL tubes using a multichannel pipette. The solutions were vortexed gently and then preincubated for 5 minutes at 37°C (after removal of the plate bottom). A 20 μL aliquot of NADPH solution using a repeating pipette was placed into all the tubes to start the reaction, followed by vortexing the tubes to assure that the NADPH mixed well. The tubes were incubated for 20 minutes at 37 °C in a shaking water bath (using a 96-well plate with the bottom removed). At the end of the incubation, the samples were quenched with 200 μL of

quenching solution. The samples were capped and vigorously vortexed for 1 minute. The samples were then placed in steps 2 and 3 at -20°C for 1 h followed by centrifugation at 3,500 rpm for 15 minutes. One hundred microliters of the supernatant was transferred into a 96-well plate using a multichannel pipette for LC/MS/MS analysis.

4.5.4 Pharmacokinetic evaluation in Sprague-Dawley rats

Preparation of the standard solution: The appropriate amount of the test substance was accurately weighed, dissolved in DMSO, and prepared into a standard stock solution with a concentration of 1.00 mg/mL. Then, accurately, the appropriate amount of the standard stock solution was taken to prepare an intermediate standard solution with a concentration of 100 g/mL in DMSO. The above intermediate standard solution was serially diluted in DMSO to generate a standard series solution. Diclofenac standard solution: The appropriate amount of diclofenac reference substance was accurately weighed, dissolved in acetonitrile and diluted to prepare a standard stock solution with a concentration of 2.00 mg/mL. Before use, this stock solution was diluted with acetonitrile to a working concentration of 50 ng/mL. To 50 µL of blank plasma, 5 µL of the compound **125** standard series solution was added, followed by the addition of 300 µL of 50 ng/mL diclofenac solution, vortexing for 2 minutes and centrifuging at 3700 rpm for 15 minutes at 4 °C. The supernatant was removed and assayed by LC/MS/MS with an injection volume of 100 µL. To 50 µL of blank plasma, 5 µL of different concentrations of compound **125**

quality control solutions and 300 μL of 50 ng/mL diclofenac solution were added, followed by vortexing for 2 minutes and centrifuging at 3700 rpm for 15 minutes at 4 $^{\circ}\text{C}$. The supernatant was removed and 100 μL was injected and measured by LC/MS/MS. To 50 μL of plasma, 5 μL DMSO and 300 μL of 50 ng/mL diclofenac solution were added, followed by vortexing for 2 minutes and centrifuging at 3700 rpm for 5 minutes at 4 $^{\circ}\text{C}$. One hundred microliters of the supernatant was removed for measurement by LC/MS/MS. The pharmacokinetic parameters were estimated using a noncompartmental model (calculated using Phoenix WinNonlin software). The elimination half-life ($t_{1/2}$) and the area under the curve of the drug (AUC) were calculated using the following formulas, where C_t is the final sample point concentration. In the formulas, λ is the end elimination slope, which is obtained by using the slope of the straight line portion of the logarithmic plasma concentration-time curve.

$$t_{1/2} = 0.693/\lambda$$

$$AUC_{0-t} = \sum \frac{t_{i+1} - t_i}{2} (C_{i+1} + C_i)$$

$$AUC_{0-\infty} = \sum \frac{t_{i+1} - t_i}{2} (C_{i+1} + C_i) + \frac{C_n}{\lambda}$$

4.6 BALB/C mice 14-Day toxicology study

The experiment was divided into a blank group, 38L group, 38H group, 125L group and 125H group, with 10 BALB/C mice in each group. The mice were intragastrically administered the respective compound for 14 days, routine blood samples were taken for blood biochemical indicators, and liver and kidney histopathological sections were taken and pathologically

observed. **Tissue samples**, prepared at a thickness of 3 mm underwent a gradient alcohol dehydration (70%, 80%, 95%, 100%) for each 30 minutes at each concentration, two xylene bottles every 20 minutes, two paraffin wax cylinders every 12 minutes, and were then embedded, sliced 4 to microns, and baked. **Hematoxylin eosin (HE) staining:** For dewaxing, three bottles of xylene were used for 8 minutes each, then two bottles of 100% alcohol for 8 minutes per bottle, 90% alcohol, 80% alcohol, and 60% alcohol for 8 minutes each. Hematoxylin staining occurred for 4 minutes followed by cleaning with running water. Hydrochloric acid alcohol differentiation was performed for 2-3 seconds then cleaned with running water. Finally, a solution of 0.5% ammonia water was used for 20 seconds followed by cleaning with running water and observation under a microscope. For eosin staining, a 0.5% solution was applied for 1 minute, then 80% alcohol, 90% alcohol for 3-5 seconds each, 95% alcohol for 5 minutes, three bottles of 100% alcohol for 5 minutes each and two bottles of xylene for 5 minutes each. Neutral resin glue sealing was followed by light microscopy and photomicrography.

ASSOCIATED CONTENT

Supporting Information.

Characterization of synthetic compounds.

AUTHOR INFORMATION

Corresponding Author

*For Z.-R.L.: phone, +86-10-63027185; fax, +86-10-6301-7302; E-mail, lizhuorong@imb.pumc.edu.cn.

*For Z.-Y.L.: phone, +86-10-63165287; fax, +86-10-6301-7302; E-mail, zongyingl@hotmail.com.

Author Contributions

‡ S.-T. X and L. Z. contributed equally to this work.

Notes

The authors declare no competing financial interest.

ACKNOWLEDGMENT

This work was supported by Xinchang Pharmaceutical and grants from the National Science Foundation of China (81473097, 81402800) and the CAMS Innovation Fund for Medical Sciences (CIFMS, 2016-I2M-1-010). We were also particularly grateful to Da-hong Ju and Mei-jie Liu from Institute of Basic Theories, China Academy of Chinese Medical Sciences for conducting this research.

ABBREVIATIONS

BMD, bone mineral density; OC, osteoclast; OB, osteoblast; BMP-2, bone morphogenetic protein-2; SAMP-6, senescence-accelerated mouse prone 6; OVX, ovariectomized; TBV, trabecular bone volume; Papp, apparent permeability coefficient; AP-BL, apical to basolateral; TEER, transepithelial electrical resistance; LY, lucifer yellow

Journal Pre-proof

REFERENCES

1. Tanaka S. Signaling axis in osteoclast biology and therapeutic targeting in the RANKL/RANK/OPG system. *Am J Nephrol.* 2007;27:466–78.
2. NIH Osteoporosis and Related Bone Diseases National Resource Center. The surgeon general's report on bone health and osteoporosis: what it means to you. Dec, 2015. [Accessed June 6, 2017]. Available at: www.niams.nih.gov/Health_Info/Bone/SGR/surgeon_generals_report.asp.
3. Mazziotti G, Bilezikian J, Canalis E, Cocchi D, Giustina A. New understanding and treatments for osteoporosis. *Endocrine.* 2012;41:58–69.
4. Kanis JA, McCloskey EV, Johansson H, Oden A, Melton LJ, Khaltav N. A reference standard for the description of osteoporosis. *Bone.* 2008;42:467–75.
5. Teitelbaum SL. Bone resorption by osteoclasts. *Science.* 2000;289:1504–8.
6. Marcucci G, Brandi ML. Rare causes of osteoporosis. *Clin Cases Miner Bone Metab.* 2015;12:151–6.
7. Polymeris A, Michalakis K, Sarantopoulou V. Secondary osteoporosis - an endocrinological approach focusing on underlying mechanisms. *Endocr Regul.* 2013;47:137–48.
8. Camacho P, Petak S, Binkley N, et al. American association of clinical endocrinologists and American college of endocrinology clinical practice guidelines for the diagnosis and treatment of postmenopausal osteoporosis - 2016. *Endocr Pract.* 2016;22:1–42.

9. Hernlund E, Svedbom A, Ivergard M, et al. Osteoporosis in the European Union: medical management, epidemiology and economic burden. A report prepared in collaboration with the International Osteoporosis Foundation (IOF) and the European Federation of Pharmaceutical Industry Associations (EFPIA). *Arch Osteoporos*. 2013;8:136.
10. Ström O, Borgström F, Kanis JA, et al. Osteoporosis: burden, health care provision and opportunities in the EU: a report prepared in collaboration with the International Osteoporosis Foundation (IOF) and the European Federation of Pharmaceutical Industry Associations (EFPIA). *Arch Osteoporos*. 2011;6:59–155.
11. Burge R, Dawson-Hughes B, Solomon DH, Wong JB, King A, Tosteson A. Incidence and economic burden of osteoporosis-related fractures in the United States, 2005-2025. *J Bone Miner Res*. 2007;22:465–75.
12. Burns ER, Stevens JA, Lee R. The direct costs of fatal and non-fatal falls among older adults - United States. *J Safety Res*. 2016;58:99–103.
13. World Health Organization. WHO scientific group on the assessment of osteoporosis at primary health care level: summary meeting report. May 5–7, 2004. [Accessed December 27, 2017]. Available at: www.who.int/chp/topics/Osteoporosis.pdf.
14. Amso Z, Cornish J, Brimble MA. Short anabolic peptides for bone growth. *Med Res Rev*. 2016;36:579–640.
15. Fujiwara S, Hamaya E, Sato M, Graham-Clarke P, Flynn JA, Burge R. Systematic review of

- raloxifene in postmenopausal Japanese women with osteoporosis or low bone mass (osteopenia). *Clin Interv Aging*. 2014;9:1879–93.
16. Bhavnani BR, Stanczyk FZ. Pharmacology of conjugated equine estrogens: efficacy, safety and mechanism of action. *J Steroid Biochem Mol Biol*. 2014;142:16–29.
17. Sanders S, Geraci SA. Osteoporosis in postmenopausal women: considerations in prevention and treatment: (women's health series). *South Med J*. 2013;106:698–706.
18. Bilezikian JP. Combination anabolic and antiresorptive therapy for osteoporosis: opening the anabolic window. *Curr Osteoporos Rep*. 2008;6:24–30.
19. Cosman F, Crittenden DB, Adachi JD, et al. Romosozumab treatment in postmenopausal women with osteoporosis. *N Engl J Med*. 2016;375:1532–43.
20. Clark EM, Durup D. Inflammatory eye reactions with bisphosphonates and other osteoporosis medications: what are the risks? *Ther Adv Musculoskelet Dis*. 2015;7:11–6.
21. Gatti D, Adami S, Viapiana O, Rossini M. The use of bisphosphonates in women: when to use and when to stop. *Expert Opin Pharmacother*. 2015;16:2409–21.
22. Wong A, Eloy JA, Couldwell WT, Liu JK. Update on prolactinomas. Part 2: treatment and management strategies. *J Clin Neurosci*. 2015;22:1568–74.
23. Kreutle V, Blum C, Meier C, et al. Bisphosphonate induced hypocalcaemia - report of six cases and review of the literature. *Swiss Med Wkly*. 2014;144:w13979.
24. Piscitelli P, Auriemma R, Neglia C, Migliore A. Alendronate: new formulations of an old and

- effective drug to improve adherence avoiding upper gastrointestinal side effects. *Eur Rev Med Pharmacol Sci*. 2014;18:3788–96.
25. Cairoli E, Zhukouskaya VV, Eller-Vainicher C, Chiodini I. Perspectives on osteoporosis therapies. *J Endocrinol Invest*. 2015;38:303–11.
26. Feehan J, Saedi A, Duque G. Targeting fundamental aging mechanisms to treat osteoporosis. *Expert Opin. Ther. Targets*. 2019;23:1031–39.
27. Ali IHA, Brazil DP. Bone morphogenetic proteins and their antagonists: current and emerging clinical uses. *British Journal of Pharmacology*. 2014;171:3620–32.
28. Li X, Yang J, He X, et al. Identification of upregulators of BMP2 expression via high-throughput screening of a synthetic and natural compound library. *J Biomol Screen*. 2009;14:1251–6.
29. Liu ZY, He XB, Yang ZY, et al. Synthesis and evaluation of 1-(benzo[b]thiophen-2-yl)ethanone analogues as novel anti-osteoporosis agents acting on BMP-2 promotor. *Bioorg Med Chem Lett*. 2009;19:4167–70.
30. Guo HF, Shao HY, Yang ZY, et al. Substituted benzothiophene or benzofuran derivatives as a novel class of bone morphogenetic protein-2 up-regulators: synthesis, structure-activity relationships, and preventive bone loss efficacies in senescence accelerated mice (SAMP6) and ovariectomized rats. *J Med Chem*. 2010;53:1819–29.
31. Li Z, Guo H, Si S, et al. Benzo 5-membered unsaturated heterocyclic compounds and

- preparation methods thereof, World Patent WO2012068702 (A1)
32. Xue ST, Guo HF, Liu MJ, et al. Synthesis of a novel class of substituted benzothiophene or benzofuran derivatives as BMP-2 up-regulators and evaluation of the BMP-2-up-regulating effects *in vitro* and the effects on glucocorticoid-induced osteoporosis in rats. *Eur J Med Chem.* 2015;96:151–61.
33. Lipinski CA. Drug-like properties and the causes of poor solubility and poor permeability. *Journal of Pharmacological and Toxicological Methods.* 2000;44:235–49.
34. Spoorendonk KM, Hammond CL, Huitema LFA, et al. Zebrafish as a unique model system in bone research: the power of genetics and *in vivo* imaging. *Journal of Applied Ichthyology.* 2010;26:219–24.
35. Xue ST, Qin W, Liu ZY. Screening on antiosteoporotic 1-(benzo[b]thiophen-2-yl)ethanone analogues on zebrafish model. *Chinese Medicinal Biotechnology.* 2015;10:211–17.
36. Artursson P, Karlsson J. Correlation between oral drug absorption in humans and apparent drug permeability coefficients in human intestinal epithelial (Caco-2) cells. *Biochemical & Biophysical Research Communications.* 1991;175:880–85.
37. Aboraia AS, Yee SW, Gomaa MS, et al. Synthesis and CYP24A1 inhibitory activity of N-(2-(1H-imidazol-1-yl)-2-phenylethyl)arylamides. *Bioorganic & Medicinal Chemistry.* 2010;18:4939–46.

FIGURE LEGENDS

Figure 1. SAR studies was performed to guide the next-step synthesis studies.

Figure 2. Structures of the compounds for the *in vivo* experiments.

Figure 3. Effects of the compounds on the bones in rats with OVX-induced osteoporosis. **(A)** Stained slices of tibia bone tissue of all groups of OVX-induced osteoporosis rats. **(B)** Effect of the tested compounds on the trabecular bone volume (TBV%) in the tibia in OVX-induced osteoporosis rats (means \pm SD, n = 10). **(C)** Representative bone density image and the processed area (square). Using OSTEOCORE 3 software, the bones of the rats were filled manually, and the bone density of each such area was calculated. **(D)** Effect of the tested compounds on BMD in OVX-induced osteoporosis rats calculated from the processed area in the bone density images (means \pm SD, n = 10). *** Probability $p < 0.001$. The p value is calculated using Dunnett's T test and differences with probability $p < 0.05$ are considered statistically significant.

Figure 4. Effect of compound **125** on the dexamethasone-induced zebrafish osteoporosis model.

(A) Images of the bone tissues of all groups of zebrafish dyed with Alizarin red. **(B, C)**

Quantification of Alizarin red staining of zebrafish bone (**B**: Staining area; **C**: Sum of optical

density) (n = 30 per group). **(D)** Expression of β -actin (internal reference protein, upper blot) and expression of target protein (BMP-2, lower blot) after treatment with **125**. **(E)** Quantification of the normalized BMP-2 signal from part **(D)**. **(F)** Relative luminescence units of **125** in p6OSE2-luc. *** Probability $p < 0.001$. * Probability $p < 0.05$. The p value is calculated using Dunnett's T test and differences with probability $p < 0.05$ are considered statistically significant.

Figure 5. BALB/C mice were administered tested compounds at a dosage of 100 or 50 (mg/kg)/day orally. **(A)** Pathological sections (250 μ m) of the livers and kidneys after 14 days of treatment. **(B, C)** Serum alanine transaminase (ALT) and aspartate transaminase (AST) levels of the indicated mice were detected to evaluate liver function (n = 10 per group). **(D, E)** Serum urea and creatinine levels of the indicated mice were detected to evaluate renal function (n = 10 per group).

Scheme 1. Synthesis of substituted benzothiophene and benzofuran derivatives. Reagents and conditions: (a) 0.1 N NaOH, H₂O, dioxane, 40 °C, 1 h, 80–83%; (b) SOCl₂, DMF, anhydrous toluene, 80 °C, 3 h; (c) Et₃N, anhydrous toluene, 0 °C–rt, 1 h, 62–86% over two steps; (d) CH₃SO₃H, EtOH, rt–50 °C, 2 h, 82–86%; (e) bromotrimethylsilane, CH₂Cl₂, 30 °C, 4 h, 70–76%; (f) 0.1 N NaOH, H₂O, 30 °C, 1 h, 85%.

FIGURES

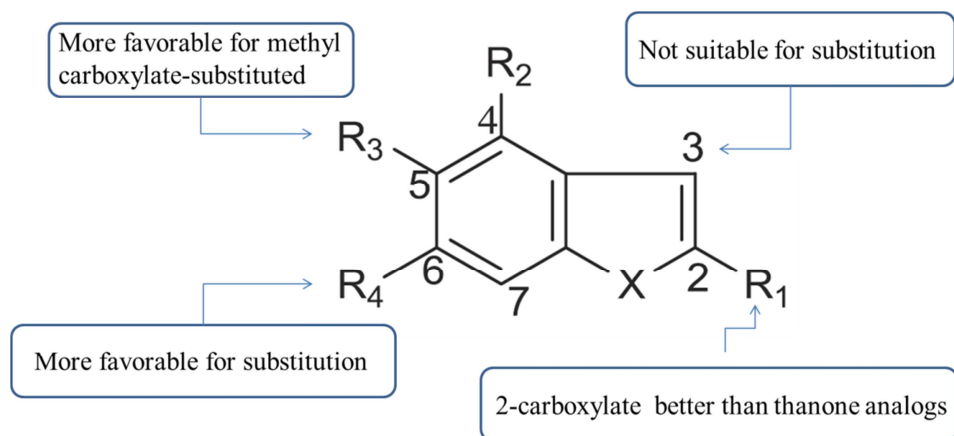


Figure 1

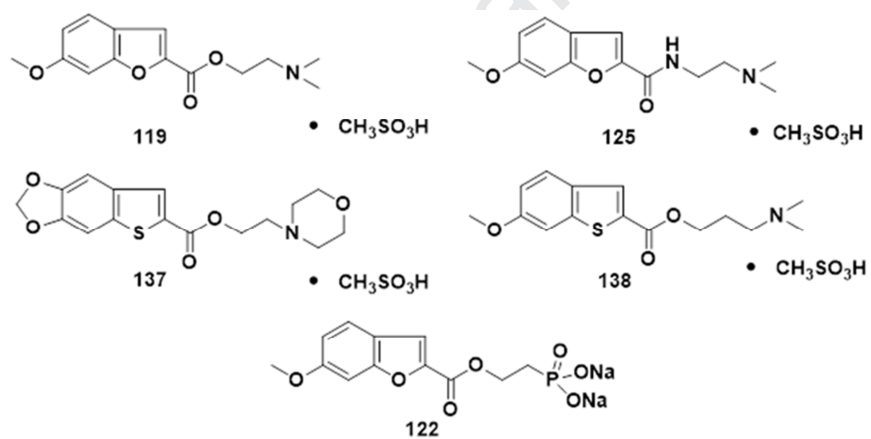


Figure 2

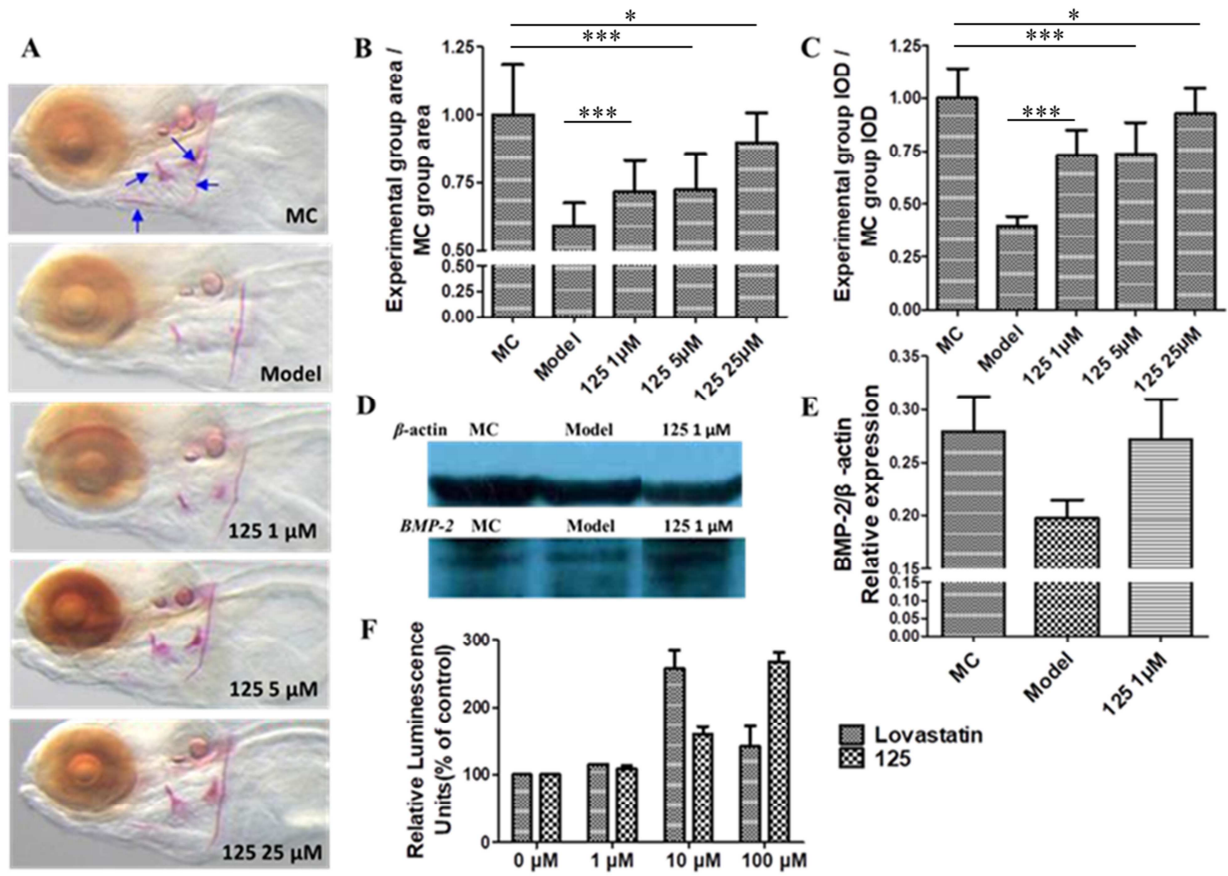


Figure 4

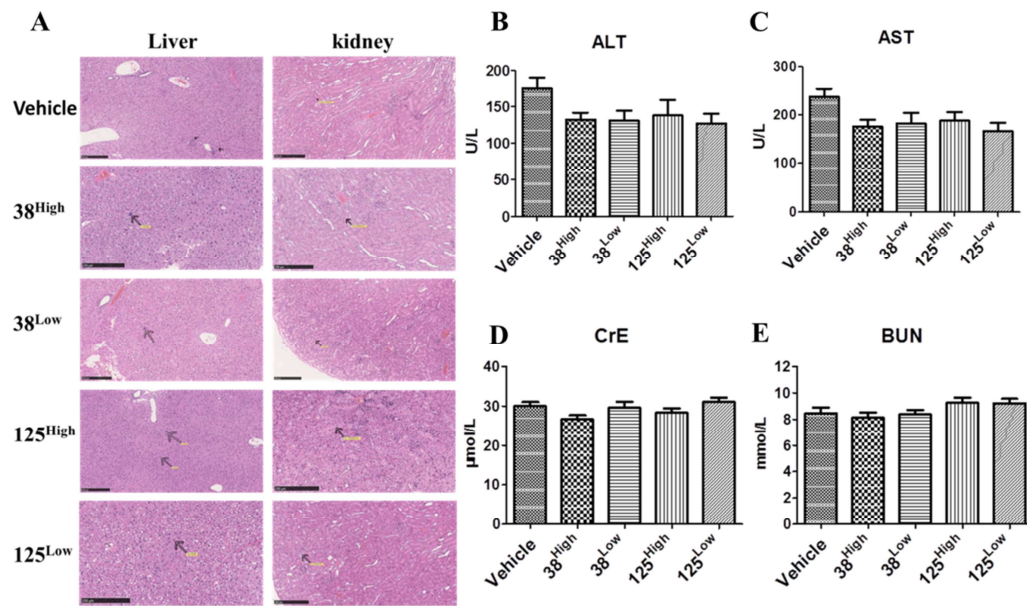
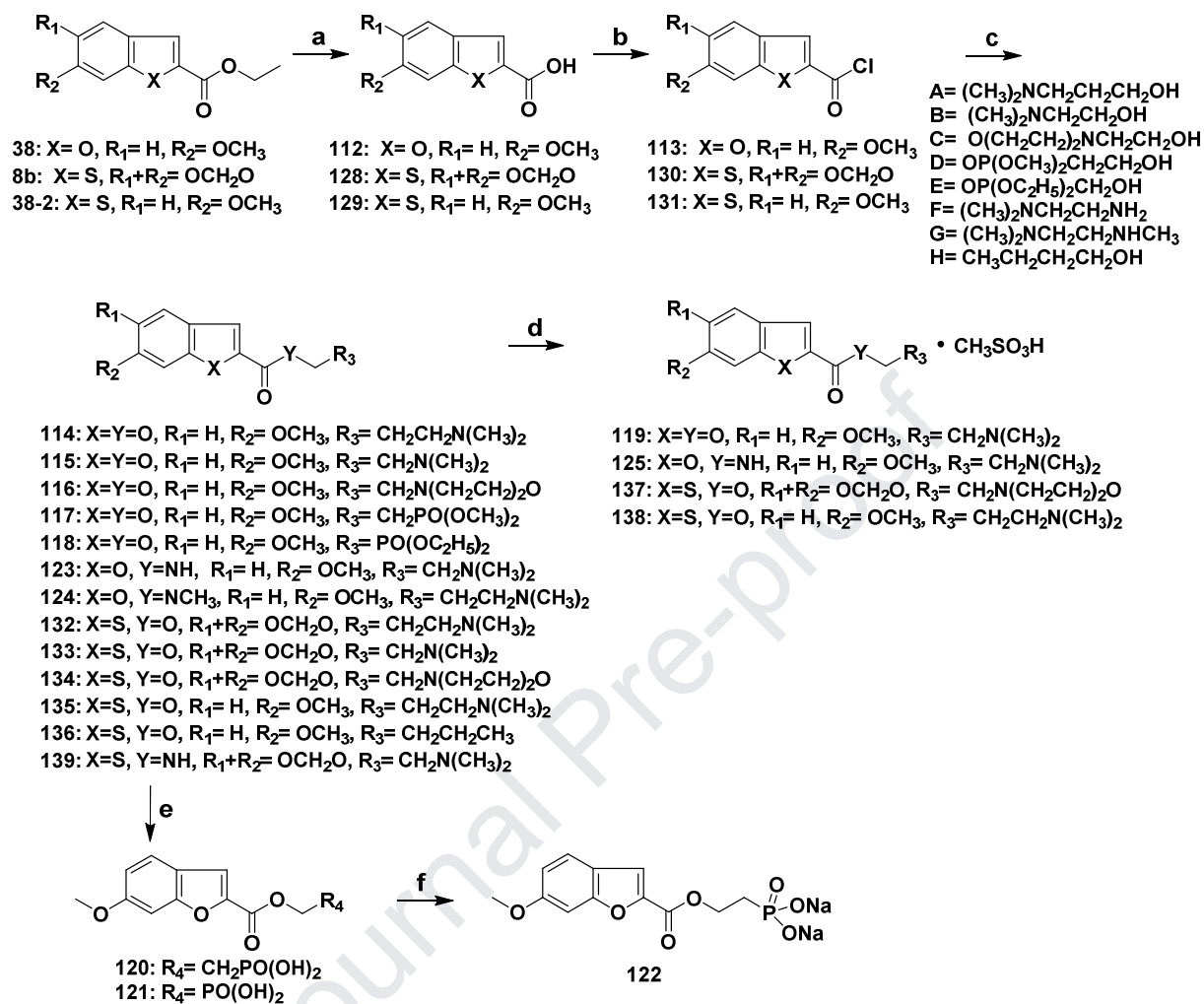


Figure 5



Scheme 1

Highlights

1. A series of benzothiophene or benzofuran analogues was synthesized and characterized.
2. **125** was considerably safe in vivo.
3. **125** can correct bone loss that is already occurring and have broad clinical applicability.
4. **125** exhibited potential for development as anabolic agents.

Journal Pre-proof

Declaration of interests

The authors declare that they have no known competing financial interests or personal relationships that could have appeared to influence the work reported in this paper.

The authors declare the following financial interests/personal relationships which may be considered as potential competing interests:

Journal Pre-proof